

# The Use of Whole Organ Decellularization for the Generation of a Vascularized Liver Organoid

Pedro M. Baptista,<sup>1\*</sup> Mohammad M. Siddiqui,<sup>2\*</sup> Genevieve Lozier,<sup>3</sup> Sergio R. Rodriguez,<sup>1,4</sup> Anthony Atala,<sup>1</sup> and Shay Soker<sup>1</sup>

A major roadblock to successful organ bioengineering is the need for a functional vascular network within the engineered tissue. Here, we describe the fabrication of three-dimensional, naturally derived scaffolds with an intact vascular tree. Livers from different species were perfused with detergent to selectively remove the cellular components of the tissue while preserving the extracellular matrix components and the intact vascular network. The decellularized vascular network was able to withstand fluid flow that entered through a central inlet vessel, branched into an extensive capillary bed, and coalesced into a single outlet vessel. The vascular network was used to reseed the scaffolds with human fetal liver and endothelial cells. These cells engrafted in their putative native locations within the decellularized organ and displayed typical endothelial, hepatic, and biliary epithelial markers, thus creating a liver-like tissue *in vitro*. Conclusion: These results represent a significant advancement in the bioengineering of whole organs. This technology may provide the necessary tools to produce the first fully functional bioengineered livers for organ transplantation and drug discovery. (HEPATOLOGY 2011;53:604-617)

Within the past 2 decades, most of the major achievements in tissue engineering have focused on tissues constructed using thin sheets of cells, such as bladder, skin, and arteries.<sup>1-3</sup> Construction of thicker tissues, such as muscle and liver, has not been possible due to limited diffusion of nutrients and oxygen within the engineered tissue mass.<sup>4</sup> It is known that cells can only survive within an area

approximately 1-3 millimeters away from a source of nutrients and oxygen,<sup>5</sup> and attempts to engineer tissues thicker than this limit have been hampered by eventual necrosis of the cells within the core of the construct.

Solid organs have an intricate vascular tree, which, through a series of branching vessels, forms a pervasive capillary network that ensures that all cells in the organ are no more than ~1 mm from a nutrient and oxygen source. Researchers have used various techniques in polymer biochemistry and scaffold design<sup>6-8</sup> to mimic the structure of this vascular network in engineered tissues. Strategies have included the coseeding of endothelial cells that spontaneously form capillary-like networks, and the engineering of branching channels to mimic the vascular tree.<sup>9,10</sup> In addition, researchers have attempted to induce angiogenesis within engineered tissues by incorporating angiogenic peptides and growth factors into scaffolds and by engineering cells used in the organ constructs to express these factors. However, these efforts have fallen short of producing scaffolds that contain a vascular tree with centralized inlet and outlet vessels that are suitable for transplantation and capable of nutrient and gas exchange.

A significant advancement in the field of bioscaffold design has been the utilization of decellularized tissue as the three-dimensional scaffold in tissue engineering strategies.<sup>11</sup> Our laboratory has previously reported the successful decellularization of porcine aortas and

Abbreviations: CK, cytokeratin; DAPI, 4,6-diamidino-2-phenylindole; ECM, extracellular matrix; FBS, fetal bovine serum; G, gauge; GFP, green fluorescent protein; hFLC, human fetal liver cell; hUVEC, human umbilical vein endothelial cell; sGAG, sulfated glycosaminoglycan.

From <sup>1</sup>Wake Forest Institute for Regenerative Medicine, Wake Forest University School of Medicine, Winston-Salem, NC; <sup>2</sup>Harvard-MIT Division of Health, Science, and Technology, Cambridge, MA; <sup>3</sup>Rice University, Houston, TX; and <sup>4</sup>Instituto Mexicano del Seguro Social, Division of Surgical Research, Guadalajara, Mexico.

Received March 11, 2010; accepted October 28, 2010.

\*These authors contributed equally to this study.

For this project, P.M.B. was supported by a predoctoral fellowship from Fundação para Ciência e Tecnologia (SFRH/BD/11802/2003), Portugal. Fellowship funding to M.M.S. was provided by the Howard Hughes Medical Institute.

Address reprint requests to: Shay Soker, Ph.D., Wake Forest Institute for Regenerative Medicine, Wake Forest University School of Medicine, Medical Center Boulevard, Winston-Salem, NC 27157. E-mail: ssoker@wfubmc.edu; Fax: 336-713-7290.

Copyright © 2010 by the American Association for the Study of Liver Diseases.  
View this article online at [wileyonlinelibrary.com](http://wileyonlinelibrary.com).

DOI 10.1002/hep.24067

Potential conflict of interest: Nothing to report.

Additional Supporting Information may be found in the online version of this article.

urinary bladder submucosa for use as scaffolds for cell seeding.<sup>2,12</sup> These decellularized aortas were seeded with endothelial progenitor cells and implanted into sheep, and the neovessels remained patent for more than 4 months.<sup>2</sup> However, effective decellularization of thicker organs and tissues has been very difficult to achieve due to inefficient penetration of the decellularization solution into the organ. More recently, Ott et al. have developed a more effective method for organ decellularization.<sup>13</sup> They have shown that by perfusing a detergent solution through the vascular network rather than relying on agitation and diffusion alone, the entire mouse heart could be decellularized and used as a scaffold for tissue engineering. However, cell seeding of three-dimensional, naturally derived scaffolds presents additional challenges.<sup>14</sup> For example, to achieve a recellularized human liver adequate for clinical use, one needs to transfer approximately  $10 \times 10^{10}$  liver cells into the scaffold. So far, such a task has not been successfully achieved. Although perfusion bioreactors have been developed to address cell seeding problems,<sup>15,16</sup> cell seeding across the entire thickness of the scaffold has been limited due to the lack of intrasc scaffold channels.

The goal of our study was to develop a novel scaffold that human liver cells could readily enter in order to repopulate the scaffold volume. We report the production of such a scaffold via a decellularization process that preserves the macrovascular skeleton of the entire liver while removing the cellular components. The intact vascular tree is accessible through one central inlet, which branches into a capillary-like network and then reunites into one central outlet. Human fetal liver and endothelial cells were perfused through the vasculature and were able to repopulate areas throughout the scaffold by engrafting into their putative natural locations in the liver. These cells displayed typical endothelial, hepatic and biliary epithelial markers, thus creating a liver-like tissue *in vitro*. This technology may provide important tools for the creation of a fully functional bioengineered liver that can be used as an alternative for donor liver transplantation.

## Materials and Methods

**Liver Preparation.** Livers were dissected from cadavers of different animal species. Dissection was carried out in a similar fashion in mice, rats, ferrets (*Mustela putorius*), rabbits, and pigs. After the animals were euthanized, a longitudinal abdominal incision was made and the liver was visualized. The portal vein was dissected and transected. The falciform and cardiac

ligaments were transected and the liver mobilized to visualize the inferior vena cava. The vena cava was transected above and below the liver and any remaining attachments to the liver were dissected. The liver was removed with the capsule intact. One side of the vena cava was ligated and the other end was cannulated with a 22-gauge (22G) cannula in mice, 20G in rats and ferrets, and size 16 tubing in rabbits and pigs. The portal vein was cannulated with a 20G cannula in rats, ferrets, and rabbits, and with size 16 tubing in pigs. All cannulae were obtained from Terumo Medical Corp., Elkton, MD and the tubing was obtained from Masterflex, Cole-Palmer Instrument Co., Vernon Hills, IL.

**Decellularization.** The cannulae in the portal veins were attached to a pump (Masterflex L/S peristaltic pump with Masterflex L/S easy load pump head and L/S 16G tubing, Cole-Palmer Instrument Co., Vernon Hills, IL) and distilled water was perfused through the portal vein at a rate of approximately 5 mL/minute (rat and ferret livers). Approximately 40 times the volume of the liver was perfused through this circuit. Subsequently, 1% Triton-X 100 with 0.1% Ammonium Hydroxide (Sigma-Aldrich) was perfused through the livers to decellularize the organ. Approximately 50 times the volume of the liver was circulated through the vascular tree. Finally, a distilled water wash was circulated to wash out the decellularization detergent.

**Bioscaffold Characterization.** DNA was isolated from a small piece from 6 different ferret bioscaffolds and three different fresh ferret livers using the DNeasy Tissue kit (Qiagen Inc., Valencia, CA) according to the manufacturer's instructions. Similar masses of scaffold and control liver tissue were used. Hematoxylin and eosin (H&E), trichrome (Newcomer Supply, Middleton, WI), and Russel-Movat Pentachrome (American MasterTech Scientific Inc, Lodi, CA) staining were performed for ferret scaffold characterization after fixation, paraffin embedding and sectioning. Collagen, sGAG and elastin quantification ( $n = 3$  samples) were performed as directed in the protocols associated with the Sircol, Blyscan and Fastin assay kits (Biocolor, Ltd., Newtownabbey, UK), respectively. A Student's *t* test were performed to compare the total amount of sGAG, O-sGAG, and elastin in fresh liver and bioscaffold samples. Ferret liver bioscaffold samples were prepared for scanning electron microscopy by lyophilizing the decellularized scaffold and cutting it into multiple sections. Ferret bioscaffold ECM components were analyzed by denaturing SDS-polyacrylamide gel electrophoresis and Western blot. Briefly, up to 70  $\mu$ g of total protein extract ( $n = 3$ ) were separated on a 4%-20% Tris-glycine gel (Invitrogen Corp., Carlsbad, CA) and

blotted onto a Immobilon-P PVDF Membrane (Millipore Corp., Billerica, MA). The membranes were blocked in 5% nonfat milk (Nestle Carnation Instant Nonfat Dry Milk; Nestle USA, Inc., Solon, OH) in TBST for 1 hour, and incubated overnight with primary antibodies, including anti-collagen I, III and IV (Southern Biotech, Birmingham, AL), anti-laminin (Sigma-Aldrich), anti-decorin (Abcam Inc., Cambridge, MA), anti-fibronectin and anti- $\beta$ -actin (Santa Cruz Biotechnology, Santa Cruz, CA), followed by appropriate horseradish peroxidase-conjugated secondary antibodies. Wet membranes were incubated with Pierce ECL Western blotting substrate (Thermo Scientific, Rockford, IL) for 1 minute and scanned in a Fujicolor LAS-3000 system (Fujifilm USA, Inc.). As positive control for protein expression, protein standards containing collagen I and III (BD Biosciences, San Jose, CA), collagen IV, fibronectin and decorin (Sigma-Aldrich) at known concentrations were loaded simultaneously on the gel. Immunohistochemical analyses were performed in formalin fixed and paraffin embedded bioscaffold and human liver sections using the same antibodies indicated above.

**Biodegradation Assay.** Decellularized ferret liver matrices were dried by lyophilization and divided into segments of 4-6 mg by mass ( $n = 3$  per time point). The segments were placed in 37°C PBS. Controls were maintained in PBS, whereas experimental samples were placed in 1 mg/mL (250 U/mL) collagenase II (Worthington Biochemical Co., Lakewood, NJ). Samples were then collected and dried again by lyophilization. The masses of the bioscaffold segments in the control and experimental samples were measured at 3, 6, 12, 24, and 48 hours of exposure collagenase and mass average and standard deviation were calculated for each time point.

**Vascular Tree Imaging.** Fluoroscopy was carried out in a decellularized pig liver using a Siemens SIRE-MOBIL Compact L C-arm. Conray Iothalamate Meglumine (Mallinckrodt Inc., St Louis, MO) contrast agent was diluted at a ratio of 1:50 in distilled water and perfused through the vasculature at a rate of 30 mL/minute. Fluorescent microscope imaging of the capillary tree ( $n = 3$ ) was obtained by perfusing 100  $\mu$ g/mL fluorescein bound to 250 kDa dextran (Sigma-Aldrich) into the mouse liver bioscaffold. Dextran bound fluorescein was used so as to minimize diffusion of the fluorescein outside of the vasculature. A fluorescent light microscope was used to obtain the other single plane images. For three-dimensional reconstruction of the vascular network, sequential pictures were taken of the bioscaffold after injection of dextran bound fluorescein particles with a Nikon 600N confocal microscope (Nikon Inc., Melville, NY). The pictures were

rendered for three-dimensional reconstruction with the software Volocity (Improvision Inc., Waltham, MA).

**Bioscaffold Transplantation.** The right lobe of the acellular ferret liver bioscaffold was sterilized using a gamma irradiator (J. L. Shepherd and Associates, Inc., San Fernando, CA) to provide a dose of 1.5 Mrad. Prior to transplantation, 150 U of heparin sodium (Abbott Laboratories, Inc., Abbott Park, IL) was injected into the bioscaffold using its portal catheter. After heparin injection, the catheter was removed and all the suture lines holding it to the bioscaffold removed. Three month old adult Sprague-Dawley rats ( $n = 3$ ) (Charles RIVER Laboratories, Inc., Wilmington, MA) were used for the intra-abdominal ectopic transplantation experiments and kept under isoflurane gas anaesthesia during the procedure. Both portal vein and vena cava of the bioscaffold were end-to-side anastomosed, respectively, with the superior mesenteric vein and the native vena cava of the host rat with 9-0 proline sutures. (Ethicon, Inc.), using a microsurgery microscope (Carl Zeiss, Inc., Jena, Germany). Vascular clamps were removed and blood was allowed to flow freely through the bioscaffold until major clotted areas could be observed. All animal procedures and handling were approved by the Institutional Animal Care and Use Committee of Wake Forest University School of Medicine, Winston-Salem, NC.

**Endothelial Cell Seeding and Bead Perfusion in the Bioscaffold.** Approximately  $100 \times 10^6$  mouse GFP-labeled endothelial cells (MS1)<sup>17</sup> were injected through vena cava of a ferret bioscaffold and allowed to attach for 2 hours at 37°C. Dulbecco's modified Eagle medium with 10% FBS and penicillin and streptomycin (Invitrogen Corp., Carlsbad, CA) was then continuously perfused for 3 days at 5 mL/minute ( $n = 2$ ). The same experiment was repeated using the portal vein as the route of entry for the MS1 endothelial cells ( $n = 2$ ). After 3 days, bioscaffolds were retrieved for fluorescent microscope analysis. In another set of experiments, bioscaffolds that were seeded through the portal vein were coinjected through the vena cava with polyvinyl beads ( $\sim 5 \mu\text{m}$ ) labeled with phycoerythrin (Wake Forest University Nanotechnology Labs, Winston-Salem, NC). The bioscaffolds were flash frozen with liquid nitrogen and cryosectioned in 20  $\mu\text{m}$  sections. These sections were stained for nuclei with 4,6-diamidino-2-phenylindole (DAPI; Sigma-Aldrich) and photographed by AxioCam in fluorescence microscope (Carl Zeiss, Inc., Jena, Germany).

**Bioscaffold Seeding with hUVECs and hFLCs.** Approximately  $70 \times 10^6$  hFLCs (isolated from 4 different human fetal livers at 17-21 weeks of gestation, as

described by Schmelzer et al.<sup>18</sup> and  $30 \times 10^6$  hUVECs (all from the same batch) were coseeded through the portal vein of ferret bioscaffolds ( $n = 4$ ) by perfusion with Advanced RPMI with 10% FBS, 1% antibiotics (Invitrogen, Corp., Carlsbad, CA), dexamethasone 0.04 mg/L, cAMP 2.45/L, hProlactin 10 IU/L, hGlucagon 1 mg/L, niacinamide 10 mM,  $\alpha$ -lipoic acid 0.105 mg/L, triiodothyronine 67 ng/L (Sigma-Aldrich), hEGF 40 ng/mL (R&D Systems, Inc., Minneapolis, MN), hHDL 10 mg/L (Cell Sciences, Canton, MA), hHGF 20 ng/mL, and hGH 3.33 ng/mL (eBiosciences, San Diego, CA). The cells were coinjected through the portal vein over a period of 16 hours with the peristaltic pump set to 3 mL/minute for effective perfusion seeding. Once seeding was completed, the peristaltic pump was set to 0.5 mL/minute for constant perfusion of the liver construct with the culture medium described above (with 1% FBS only) and for the first 48 hours with matrigel 3 mg/250 mL dissolved on it (BD Biosciences, San Jose, CA). Culture medium was changed every 48 hours and samples were taken for urea secretion analysis. After 1 week, a small piece of the seeded scaffold was collected for DNA extraction and the remaining bioscaffold was fixed in 4% paraformaldehyde and processed for paraffin embedding (Thermo Scientific, Rockford, IL). Histological analysis was performed using H&E staining in 5  $\mu$ m bioscaffold sections and immunofluorescence with anti-albumin, *Ulex europaeus*-I lectin, and anti-fibroblast (Sigma-Aldrich), anti-EpCAM, anti-CYP3A, anti-CYP2A, anti-cytokeratin 19, anti-cytokeratin 18, anti-CD34, anti- $\alpha$ SMA (Santa Cruz Biotechnology Inc., Santa Cruz, CA), anti-hepatocyte specific antigen (Hep-1), anti-Von Willebrand Factor, anti- $\alpha$ -fetoprotein, anti-Ki67 (Dako Inc., Carpinteria, CA), anti-eNOS, anti-CD45 (BD Biosciences, San Jose, CA), anti-macrophage (Acris Antibodies, GmbH, Herford, Germany) antibodies. Appropriate secondary antibodies labeled with Alexa Fluor 633 and Texas Red or Rhodamine were used. YO-PRO1 (Invitrogen, Corp., Carlsbad, CA) was used for nuclear staining. A LSM510 confocal microscope (Carl Zeiss, Jena, Germany) was used for the images. For proliferation and apoptosis analysis, anti-Ki67 (BD Biosciences, San Jose, CA) antibody and TdT In Situ Apoptosis Detection Kit (R&D Systems Inc., Minneapolis, MN) were used. Five images were taken with the LSM510 confocal microscope of different areas of the seeded liver bioscaffolds ( $n = 3$ ) for each staining and image analysis software SigmaScan Pro 5.0 (Aspire Software International, Ashburn, VA) was used for quantification. Urea and albumin secreted into the culture medium

were detected with the QuantiChrom Urea Assay Kit (BioAssay Systems, Hayward, CA) and human albumin ELISA kit (Bethyl Laboratories, Inc., Montgomery, TX), respectively, and normalized against the total DNA extracted from the seeded liver bioscaffold and from the hFLCs controls in petri dishes. Prostacyclin (PGI<sub>2</sub>) secretion by the EC cells was induced by adding 100nM of bradykinin (Sigma-Aldrich) to the culture medium. Samples were taken at 3 and 6 hours and 6-keto-PGF<sub>1 $\alpha$</sub>  was measured using an ELISA kit (Assay Designs Inc., Ann Arbor, MI) and normalized against the total DNA extracted from liver constructs and EC controls in petri dishes.

**Platelet Deposition Studies.** Seeded ferret bioscaffolds were retrieved after 7 days in the bioreactor were retrieved and perfused with freshly harvested heparinized rat blood. Nonseeded bioscaffolds were used as controls. After 30 minutes incubation with blood, the bioscaffolds were rinsed for 30 minutes with Krebs-Ringer Lactate buffer (Sigma-Aldrich) and immediately fixed in 10% buffered formalin (Fisher Scientific, Co., Pittsburgh, PA). One piece of the bioscaffold was further fixed for 24 hours in 2.5% glutaraldehyde for electron microscopy. Liver sections were imaged with a transmission electron microscope (Royal Philips Electronics Inc., the Netherlands). The remaining bioscaffold was processed for histology. Sections (20  $\mu$ m thick) were stained for platelets with anti-integrin  $\alpha$ IIb antibody (Santa Cruz Biotechnology Inc., Santa Cruz, CA) and anti-mouse alexa fluor 633 secondary antibody. Cell nuclei were stained with YO-PRO1 (Invitrogen, Corp., Carlsbad, CA). The stained tissue was imaged with LSM510 confocal microscope (Carl Zeiss, Jena, Germany) and 4 pictures from each section were taken. Average fluorescence from stained platelets was quantified in each picture with image analysis software SigmaScan Pro 5.0 (Aspire Software International, Ashburn, VA).

## Results

**Perfusion Decellularization of Cadaveric Livers.** Previous studies have shown that decellularization of thick tissues, such as liver, could be achieved only if the tissue was sectioned into thin slices and agitated in a detergent solution, which destroyed the organ's architecture, including its vascular network.<sup>19</sup> Perfusion of Triton X-100 and ammonium hydroxide containing solution successfully decellularized the livers of various species including from mice (Fig. 1B), rats, ferrets (Fig. 1A), and adult pig. After passing the decellularization solution through the vascular network (~1

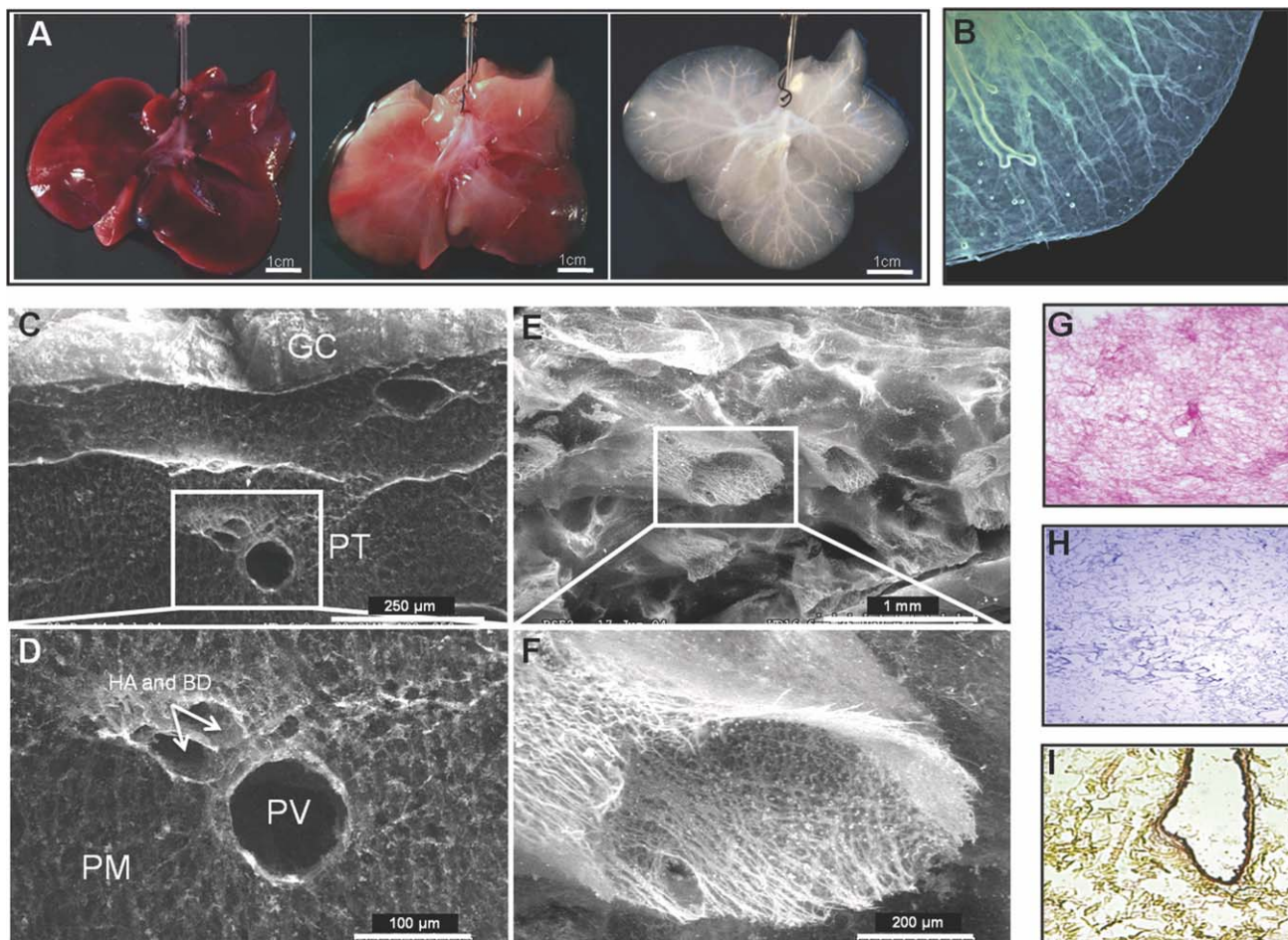


**Fig. 1.** Preparation and ultrastructural analysis of the acellular vascularized bioscaffold. Whole ferret livers were decellularized as described under “Methods”. (A) Macroscopic view of a ferret liver at 0, 20, and 120 minutes of the decellularization process. (B) A decellularized lobe of the liver demonstrating clear parenchyma, defined liver capsule and vasculature. (C) Scanning Electron Microscopy (SEM) image of a cross-section of the decellularized bioscaffold at 120 x magnification shows an intact Glisson’s capsule (GC), intact lobules and vascular structures of the portal triad (PT) (see cartoon in Fig. 4A). (D) A higher magnification image of C demonstrates intact ‘portal triad’ with portal vein (PV), hepatic artery (HA) and biliary duct (BD), and parenchymal matrix mesh (PM). (E) SEM image of a cross-section of the liver bioscaffold at the liver hilum at 40x magnification showing blood vessels constructed of woven collagen fibers and no cellular material visualized. (F) A higher magnification image of (E) further demonstrates the details of a woven structure of a blood vessel. (G) H&E staining of decellularized liver sections showing no cellular staining and pink eosinophilic staining expected from proteinous extracellular matrix. (H) Mason’s Trichrome staining of decellularized liver sections shows blue staining indicative of extracellular matrix proteins without any cellular material observed. (I) Movat-Pentachrome staining of decellularized liver sections demonstrates yellow staining for collagen with periarteriolar dark staining for elastin.

hour for mice, ~2 hours for ferrets, ~3 hours for rats, and ~24 hours for pig livers), the liver parenchyma became transparent and the vascular tree was clearly visible under low magnification microscopy (Fig. 1B). Spectrophotometric analysis indicated the removal of approximately 97% of the DNA from the tissue, confirming the efficiency of the perfusion decellularization method (Supporting Information Fig. 1A). These results were further confirmed by agarose gel electrophoresis, followed by ethidium bromide staining (Supporting Information Fig. 1B).

To evaluate whether the ultrastructure of the bioscaffold was preserved after decellularization, we examined sections by scanning electron microscopy (SEM)

(Fig. 1C-F). We observed reticular collagen fibers that provide support for the hepatic tissue (Fig. 1C). As shown in Fig. 1D, “portal triad” structures consisting of a large portal vein, bile duct, and the hepatic artery, remained intact. We observed honeycomb structures typical of the hepatic lobules surrounding the portal triad, but no remaining intact cells could be seen. Figure 1E shows multiple hollow structures at the liver hilum with intact and patent blood vessels; increased magnification revealed tightly interwoven fibers along the vessels (Fig. 1F).

**Structure and Biochemical Composition of the Liver Bioscaffold.** Histochemical staining was carried out to further characterize the composition of the

**Table 1. Quantification of the total level of collagen, elastin and sulfated glycosaminoglycans (sGAG) in the liver bioscaffold and fresh liver. Total and O-sulfated GAG amounts were measured in fresh and acellular liver bioscaffold ( $n = 3$ ). Levels of total sGAG are higher in the acellular scaffold, possibly due to the low amounts of total cellular proteins in the decellularized liver extract. The ratio between N-sulfated GAG (heparin, heparan sulfate, etc.) and O-sulfated GAG remains constant after the decellularization process. These results indicate that a large quantity of sGAG is preserved in the acellular scaffold. Collagen content in the acellular liver bioscaffold is also significantly higher than the contents reported in the literature for fresh liver (1.2%-2.5%),<sup>20,21</sup> probably due to the removal of cellular proteins in the acellular bioscaffold. Elastin amounts are lower, yet not significantly, in the acellular liver bioscaffold compared with fresh liver extracts (\*  $p < 0.05$ ).**

Parameter	Fresh Liver	Acellular Liver
Total sGAG (% of dry weight)	$0.37 \pm 0.005^*$	$0.51 \pm 0.02^*$
O-sGAG (% of sGAG)	$77.7 \pm 1.1$	$73.1 \pm 9.3$
Total collagen (% of dry weight)	(1.2-2.5)*	$7.2 \pm 1.7^*$
Total elastin (% of dry weight)	$29.0 \pm 3.4$	$23.0 \pm 8.1$

decellularized tissue extracellular matrix (ECM). H&E staining showed pink eosinophilic staining typical of collagen, whereas no basophilic staining typical of cellular nuclear material was observed (Fig. 1G). Masson's Trichrome staining confirmed these results, showing a homogeneous blue staining consistent with collagen (Fig. 1H). The H&E and Mason's Trichrome stained sections revealed multiple collagen layers with vascular channels, but with no evidence of remaining cells. Movat's Pentachrome staining of the decellularized liver tissue revealed yellow stained fibers and periarteriolar black staining, indicative of the presence of collagen and elastin fibers, respectively (Fig. 1I). There were no areas of red staining observed that would indicate cellular material. Further analysis using Alcian Blue/PAS staining showed widespread distribution of neutral glycosaminoglycans. Although some of these molecules are soluble in water, they were still present at the end of the decellularization procedure (Supporting Information Fig. 1C).

Quantification of ECM components indicated that  $7.2\% \pm 1.7\%$  of the dry weight of the decellularized liver tissue is collagen. This is significantly higher ( $P < 0.05$ ) than the quantity found in fresh liver tissue (1.2%-2.5%),<sup>20,21</sup> and may be explained by the removal of cellular proteins. Elastin was measured at  $23.0\% \pm 8.3\%$ , which does not significantly differ from fresh liver tissue (Table 1). Sulfated glycosaminoglycans (sGAG) were measured at  $0.51\% \pm 0.02\%$  of the dry weight of the decellularized tissue, compared to 0.37%

$\pm 0.01\%$  in native tissue. The difference was significant ( $P < 0.05$ ), and again may be explained by the absence of cellular components (Table 1). Finally, the level of O-sulfation was not significantly different between fresh and acellular liver tissues.

Western blot analysis showed the presence of collagens I, III, and IV; decorin; fibronectin; and laminin (Fig. 2B,C) in the decellularized liver tissue. Immunoreactive bands in the Western blot had in most of the cases a similar pattern for fresh and acellular liver tissues. Although these proteins were present in the bioscaffold, their relative amounts could not be determined due to the multiple banding patterns. No cellular cytoskeleton  $\beta$ -actin was detected (Fig. 2B,C).

Localization of specific ECM molecules in the acellular liver bioscaffold was confirmed by immunohistochemical analyses in comparison with fresh human liver tissue. In general, collagens I, III and IV, laminin and fibronectin were observed around vascular structures and parenchymal areas of the acellular liver bioscaffold (Fig. 2A). Similarly, immunostaining results of the fresh liver showed collagens I, III, and IV mostly around larger vessels, consistent with their localization in the vascular basal membrane, but also throughout the parenchymal space. Laminin expression was intense in larger vessels but was almost absent in the parenchymal space of the fresh liver and acellular scaffolds. Fibronectin had the opposite distribution, showing strong staining in the parenchymal space and lighter staining in larger vessels. Interestingly, biliary ducts and ductules were only positive for laminin, fibronectin and collagen IV in both bioscaffold and fresh liver. Image analysis revealed that the number of portal triad structures counted in the acellular liver ( $17.8 \pm 2.2$ ) were similar to the number found in fresh liver sections ( $17.0 \pm 4.7$ ) and that the staining pattern between the two samples was similar, thus indicating good preservation of ECM molecules in the bioscaffold.

Degradation of the liver bioscaffold, showed approximately 80% loss of the original mass within the first 6 hours and complete degradation by 48 hours (Fig. 2D), indicating its susceptibility to enzymatic remodeling. The mass of control bioscaffolds incubated without collagenase remained stable.

**Vascular Network Preservation and Patency.** To assess the patency of the vascular channels of the decellularized liver scaffold, we infused fluorescein-labeled 250 kDa dextran particles through the portal vein (Fig. 3A). Tracking of the particles throughout the network under low magnification fluorescent microscopy showed a defined vascular tree with multiple branching

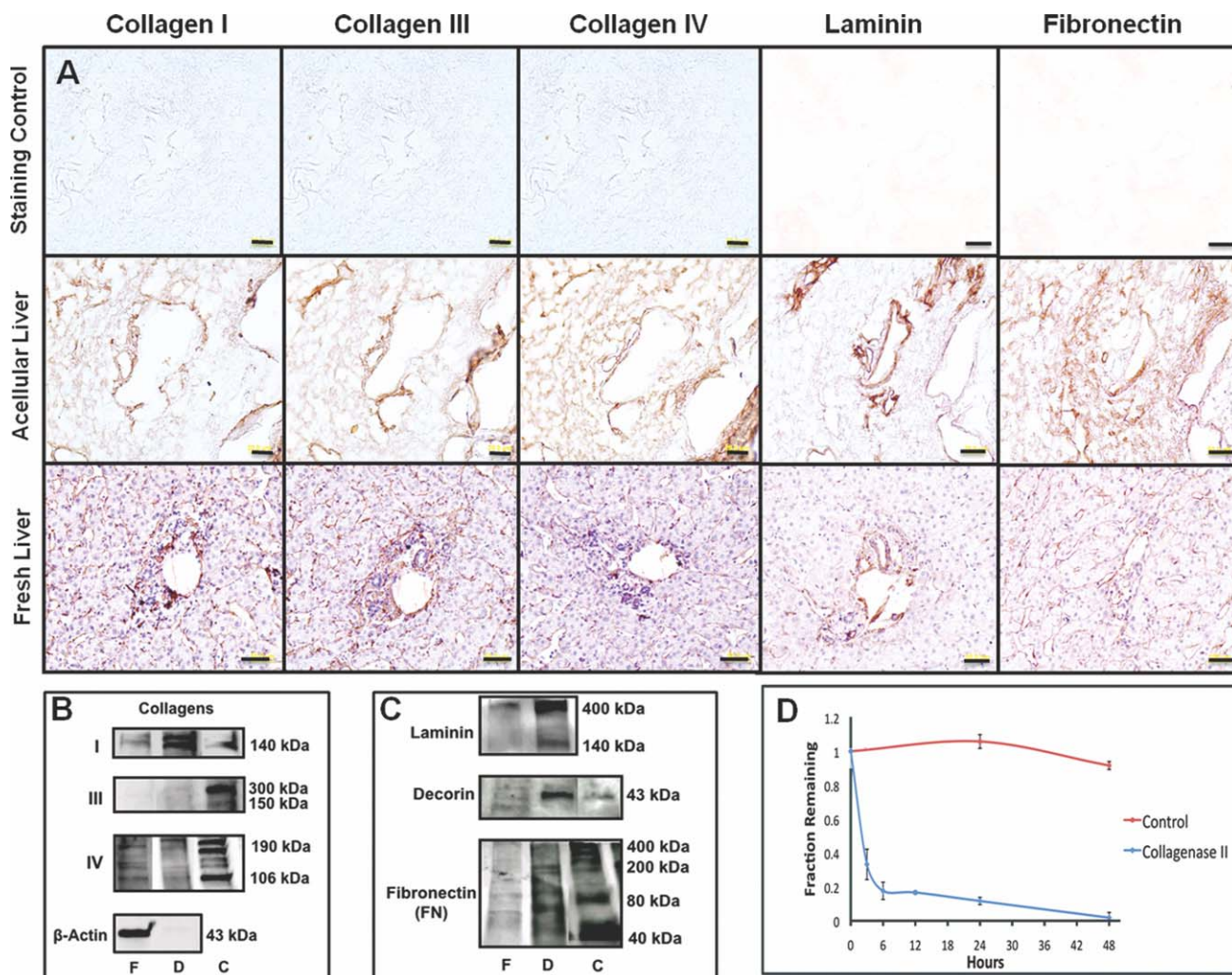
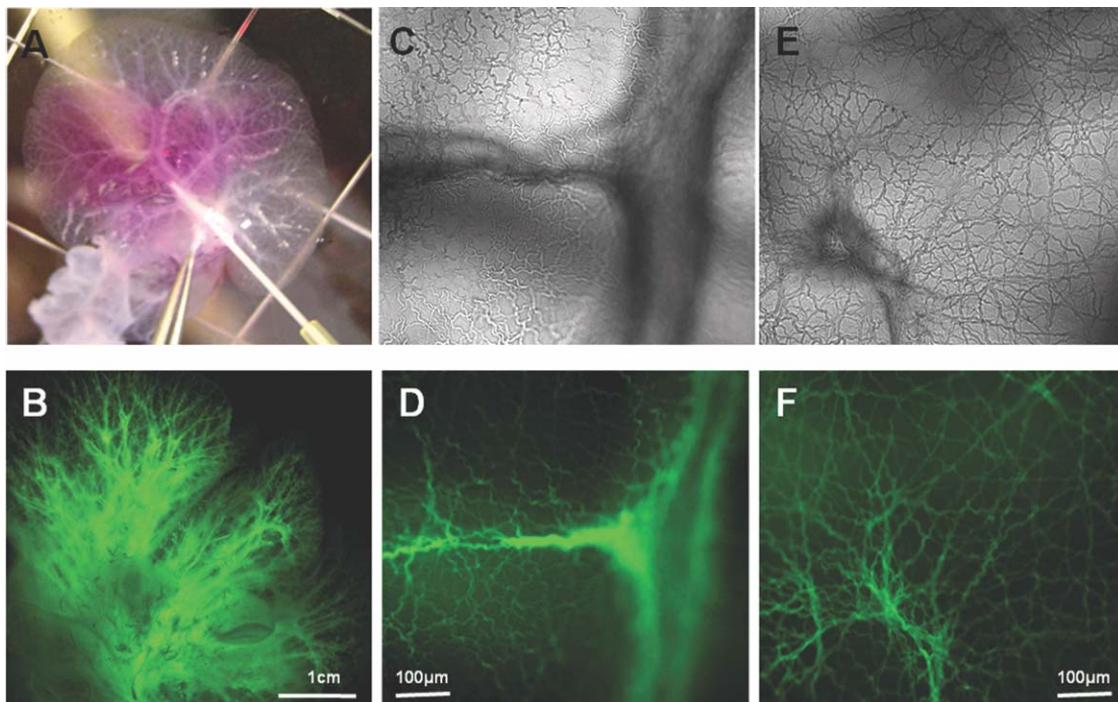


Fig. 2. Decellularized liver scaffolds preserve ECM proteins and their natural localization. Sections of decellularized and fresh ferret liver were prepared for histological, molecular and biochemical analyses, as described in “Methods”. (A) Immunostaining for collagen I, III, IV, laminin and fibronectin (as indicated) show similar distribution of these proteins in the fresh and decellularized liver bioscaffold sections. Controls were stained with isotype-matching antibodies showed no positive staining. (B, C) Scale bar = 20  $\mu$ m. Western blot analysis shows several bands (including some common degradation products) corresponding to collagen I (pro- $\alpha$ 1 at 140–210 kDa, pro- $\alpha$ 2 at 130–140 kDa) in both fresh liver and liver bioscaffold, collagen III (pro- $\alpha$ 1 at 150–200 kDa, trimer at 300 kDa) detectable only in the liver bioscaffold, laminin ( $\alpha$ 1 at 400 kDa,  $\beta$ 3 at 140 kDa), and decorin (43 kDa) observed in fresh liver (F), liver bioscaffold (D) and purified protein control (C). Fibronectin (monomer at 200 kDa, dimer at 400 kDa) and collagen IV ( $\alpha$ 1- $\alpha$ 6 at 106–190 kDa) had more extensive banding patterns, characteristic of degradation products.<sup>42</sup> No cellular  $\beta$ -actin (43 kDa) was detected in the decellularized liver, in contrast to a dense band observed in the fresh liver protein extract. (D) Collagenase II-mediated biodegradation analysis of the decellularized livers ( $n = 2$ ) was performed as described under “Methods”. A total of 50% of the bioscaffold was degraded within the first 2 hours of incubation and complete degradation was completed by 48 hours.

(Fig. 3B). At higher magnification, we observed fine branching structures, indicating that the architecture of small capillaries remained mostly intact and patent in the bioscaffold. No significant diffusion of dextran into areas that would correspond to liver parenchyma (Fig. 3C–F) was observed during most of the experiment. However, after 5–10 minutes of constant perfusion the whole acellular liver eventually became fluorescent, suggesting some leakage from the vascular channels to the parenchymal spaces. We further analyzed the fluorescently-labeled vascular network with confocal laser microscopy to reconstruct the three-

dimensional structure of the capillary network (Supporting Information Fig. 1D). We found that the bioscaffold retains a vascular network that exhibits multiple branching points with an average diameter of 15 micrometers, the size that would approximately be expected from capillaries.<sup>22</sup> To further confirm the integrity of the vascular network and to demonstrate that fluid injected into the vasculature flowed through it rather than extravasate throughout the organ, an x-ray fluoroscopic study with radio-opaque dye was performed (Supporting Information Fig. 1E,F and Supporting Information Video 1). The fluoroscopy



**Fig. 3.** Characterization of vascular patency of the liver bioscaffold. (A) Fluorescein-labeled 250 kDa dextran into the portal vein of a decellularized mouse liver, as described in “Methods” ( $n = 4$ ). (B) The decellularized mouse liver shown in A was visualized under fluorescent microscopy revealing the native vascular tree of the liver. (C, D) Large branching vasculature of the decellularized mouse liver is visualized by light and fluorescent microscopy, respectively. (E, F) An extensive network of capillary size vessels is visualized by light and fluorescent microscopy, respectively.

demonstrated that the injected dye flowed, as would be expected, inside intact vascular channels, moving slowly from larger vessels to smaller capillaries. The capillary structures appeared intact, with no obvious loss of dye into extra-vesicular areas.

To test the mechanical strength of the vascular network, unseeded liver bioscaffold was transplanted in the abdominal cavity of adult rats. The mechanical properties of the vasculature supported microsurgical suturing to the host’s blood vessels. Normal flow of blood throughout the acellular liver bioscaffold was maintained for up to 60 minutes in heparinized rats, without noticeable leakage (Supporting Information Fig. 2A,B). However, due to the bare lumen of the vascular network, clotting eventually stopped the blood flow.

**Re-Endothelialization of the Vascular Network of the Decellularized Scaffold.** Endothelial coverage of the lumen of the vasculature is essential to prevent thrombosis and to provide proper vascular function. To address this need, we compared seeding of GFP-labeled endothelial cells (ECs) through the vena cava with seeding through the portal vein (Fig. 4). We hypothesized that retrograde flow from the vena cava (Fig. 4A, gray arrow) would enter the liver lobule through the central vein and deposit cells in the peri-

central area. In contrast, cells seeded through the portal vein, in the direction of physiologic flow, would enter the lobule through the portal triad and be deposited in the periportal area (Fig. 4A, purple arrow). The results of the seeding experiments confirmed that the distribution of the cells was consistent with these predictions (Fig. 4B-D). In Fig. 4B, fluorescent EC were seeded via vena cava and then cultured under constant medium perfusion for 3 days. Fluorescent microscopy showed that the labeled EC were distributed throughout the larger vessels concentrating in regions corresponding to central veins (Fig. 4B) and in smaller branches and capillary-size vessels. In the reciprocal experiment (Fig. 4C), GFP-labeled EC seeded through the portal vein were distributed throughout the bioscaffold, with higher concentration of cells in the periportal areas of the liver lobule. Interestingly, some of these cells were observed aligning with the flow direction of the perfused culture medium (Fig. 4C, inset). In either seeding approach the EC lined the vascular network, ranging from the larger vessels to the capillary size.

In order to test whether cells could be seeded throughout the entire vascular network, we first injected the bioscaffold with EC via portal vein and subsequently injected red fluorescent beads via the

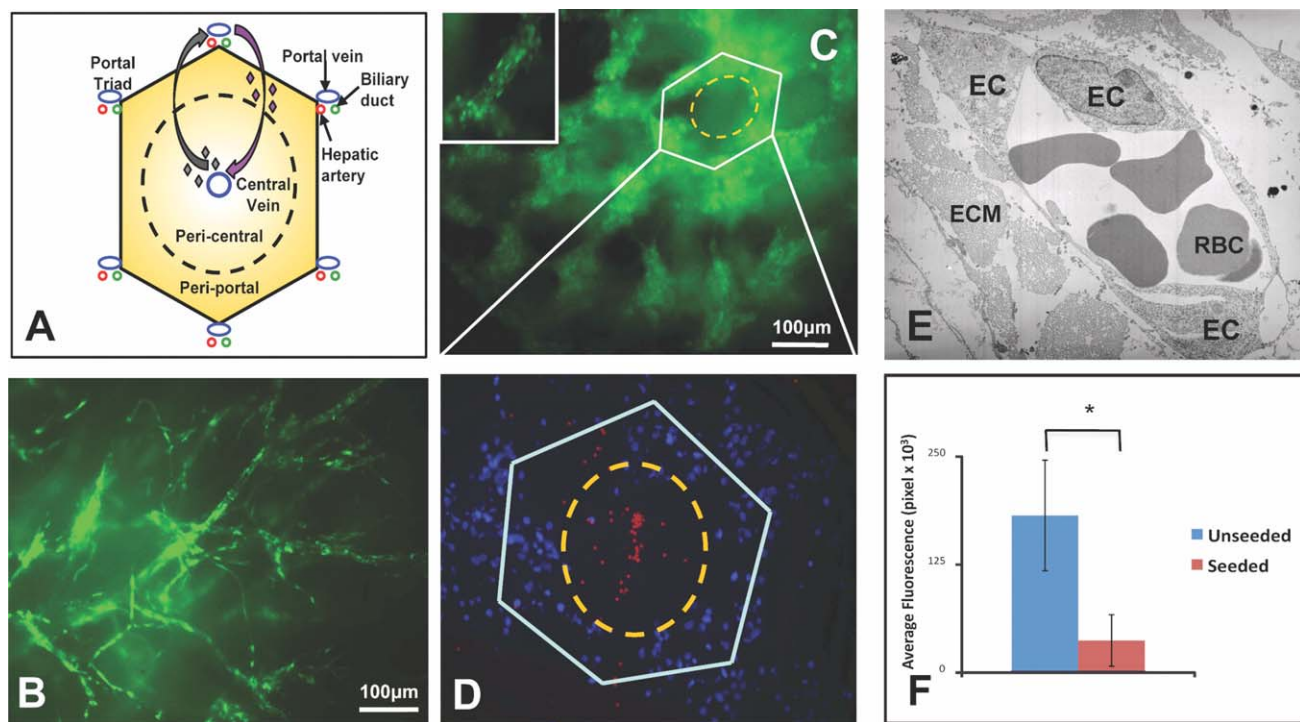


**Fig. 4.** Re-endothelialization of the ferret liver bioscaffold. Decellularized ferret liver bioscaffolds were seeded with GFP-labeled ECs, as described in Methods ( $n = 2$ ). (A) Schematic representation of the liver lobule with its hexagonal shape. The yellow gradient represents the progressive cellular zonation from periportal space to the pericentral area (dashed circle). The gray arrow represents retrograde flow direction from the vena cava and the purple arrow represents the physiologic flow direction of from the portal vein. The diamond shapes represent the seeded cells. (B) GFP-labeled ECs seeded from the vena cava are lining the bioscaffold's vascular channels. (C) GFP-labeled ECs seeded from the portal vein are distributed predominantly in the periportal areas. A higher magnification (insert) shows that several endothelial cells are needed to cover the lumen circumference and some of them are aligned in the direction of the flow of the medium. (D) Coseeding of fluorescently-labeled beads (red) through the vena cava and ECs (DAPI staining blue) through portal vein. The fluorescent beads are distributed in the core of the liver lobules (dashed circle) and the endothelial cells are localized in the periportal area (hexagon). (E) Transmission electron micrograph showing the lumen of a vascular channel covered with EC and red blood cells inside. ECM fibers are observed around the ECs. (F) The platelet staining in Supporting Fig. 3B,C and Supporting Fig. 4 was quantified and average fluorescence was calculated. Statistically significant difference ( $P = 0.006$ ) in platelet detection (fluorescence signal) observed between unseeded and re-endothelialized bioscaffolds ( $n = 3$ ).

vena cava. Fluorescent microscopy was used to visualize the DAPI-stained EC and the red fluorescent beads within the vasculature. The image in Fig. 4D clearly shows that portal vein-seeded ECs were predominantly deposited in the periportal regions of the liver lobule (Fig. 4D, hexagon), whereas vena cava-perfused beads were concentrated in the region of the central vein (Fig. 4D, dashed circle).

The resolution of the fluorescent microscopy (Fig. 4C) did not allow us to determine if the EC were able to completely cover the entire luminal surface of the vascular channels in the bioscaffold. Transmission electron microscopy (TEM) was used to achieve high-resolution analysis of ECs inside the vasculature lumen within the bioscaffold. In one section we observed 3 ECs covering the entire luminal surface of a vessel (Fig. 4E). Higher magnification showed formation of cellular junctions between two adjacent ECs (Supporting Information Fig. 3A), indicating active spreading and formation of cell-cell junctions.

ECs coverage of the vascular lumen predicts a non-thrombogenic surface and we tested this hypothesis by perfusing seeded and unseeded bioscaffolds with fresh rat heparinized blood. Platelet adhesion and aggregation to the scaffold's matrix was analyzed by immunostaining with anti-integrin  $\alpha$ IIb antibodies (Supporting Information Fig. 3B,C). A robust platelet aggregation is seen inside and around vascular structures of the unseeded bioscaffolds and, in contrast, only a small number of platelets were observed in the seeded bioscaffolds (Supporting Information Figs. 3C and 3B, respectively; Supporting Information Fig. 4). Quantification of platelet staining showed a statistically significant difference between seeded and unseeded bioscaffolds (Fig. 4F), confirming the antithrombogenic function of the ECs in the seeded bioscaffolds.

**Recellularization of the Decellularized Scaffold's Parenchyma.** We performed series of coseeding experiments of human umbilical vein endothelial cells (hUVECs) and freshly isolated human fetal liver cells

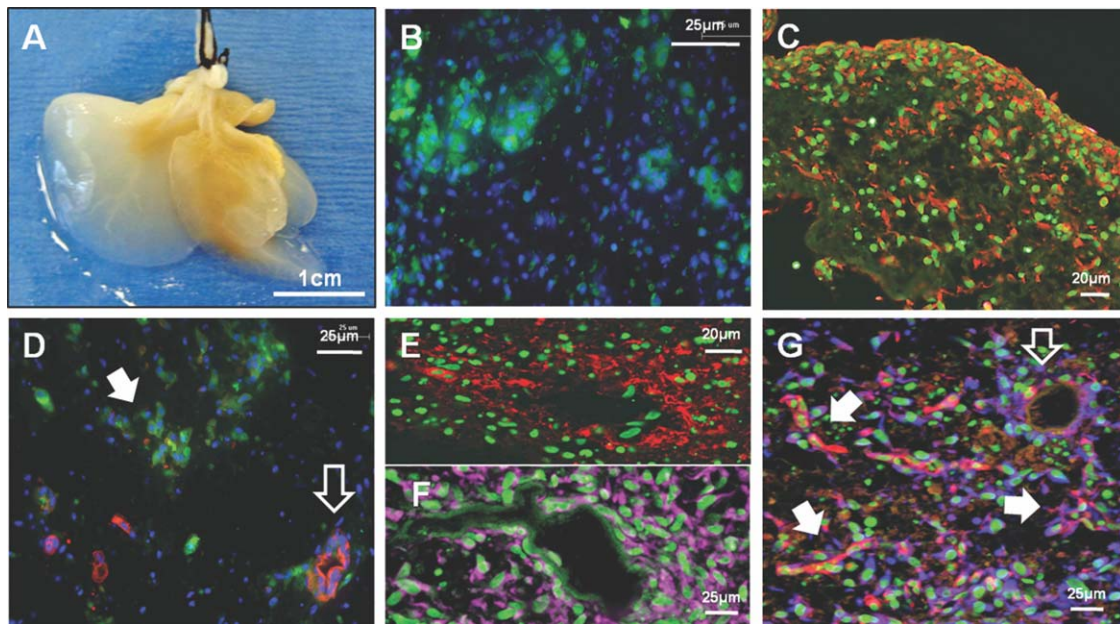


**Fig. 5.** Recellularization of the liver bioscaffold's parenchyma. Decellularized ferret liver bioscaffolds were seeded with hFLCs and hUVECs, as described in "Methods" ( $n = 4$ ). (A) Macroscopic appearance of a right lobe of a ferret liver bioscaffold 7 days after seeding. (B, C) Immunofluorescence staining P450 CYP2A (green) and P450 CYP3A (red), respectively, reveal hFLCs engraftment throughout the liver bioscaffold. (D) Staining for cytokeratin 19 (red) and albumin (green) shows a biliary tubular structure (arrow) staining intensely for cytokeratin 19 and clusters of cells staining green (solid arrow) for albumin. (E, F) Staining for Von Willebrand Factor (vWF) (red) and endothelial nitric oxide synthase (eNOS) (pink) shows hUVECs around vascular structures. (G) Staining for *Ulex europaeus*-I lectin binding (red) and Hep-1 (blue) demonstrates specific localization of hUVECs around vascular structures (arrow) with some linear projections resembling capillaries (solid arrow) emanating from larger vessels that are surround by hFLCs expressing Hep-1. All nuclei stained with YO-PRO1 (green) or DAPI (blue).

(hFLCs), using the methods developed for re-endothelialization of the bioscaffolds. An initial indication of successful cell seeding of the bioscaffold was apparent by a macroscopic change in the bioscaffold appearance from transparent white to opaque yellow 3–4 days after seeding (Fig. 5A). DNA extraction from a small sample of the seeded scaffold after 7 days revealed a 10-fold increase in DNA concentration ( $P = 0.0061$ ) compared to an acellular scaffold (Supporting Information Fig. 1A). These DNA amounts correspond to approximately 37% of the DNA present in fresh ferret liver. H&E staining showed dense cellularity throughout the whole seeded bioscaffolds (Supporting Information Fig. 3D). Proliferation was assessed by immunofluorescence staining for Ki67 and revealed a high number of positive cells detected throughout the bioscaffold (Fig. 6A). Accordingly, TUNEL staining showed a low number of apoptotic cells (Fig. 6B). Quantitative image analysis confirmed a 3× higher number of proliferating versus apoptotic cells (Fig. 6C).

Immunofluorescence staining showed hepatocytic lineage markers such as  $\alpha$ -fetoprotein (Supporting Information Fig. 3E), CYP2A and CYP3A (Fig. 5B,C) were expressed by cells in the parenchyma. Double immunostaining showed intense staining for cytoker-

tin 19 (CK19) in biliary tubular structures throughout the bioscaffold and clusters of albumin-expressing hepatocytes distributed in the parenchyma (Fig. 5D). There was very little coexpression of these markers by the same cells, suggesting that the bioscaffold contains discrete niches for bile duct and hepatocytes. A similar pattern was observed when sections were costained with CK19 (biliary epithelial cells) and CK18 (hepatocytes) (Supporting Information Fig. 3F). CK19 cells are seen in ductal structures and clusters of CK18 cells surrounding them and in the parenchyma. Some cells showed coexpression of CK19 and CK18, suggesting an immature hepatoblast phenotype.<sup>23</sup> Endothelial cell markers such as Von Willebrand Factor (vWF) (Fig. 5E) and endothelial nitric oxide synthase (eNOS) (Fig. 5F) showed staining around the vascular structures of the bioscaffold. Finally, double staining for ECs and hepatoblasts with *Ulex europaeus*-I lectin and anti-hepatocyte specific antigen (Hep1), respectively, showed a pattern of ECs distribution in capillary structures (arrows) branching from a larger vascular structure (arrowhead) (Fig. 5G). Clusters of human hepatoblasts (blue) were observed surrounding these vascular structures but had a much broader distribution in the parenchyma. Other cell types that may have existed in the

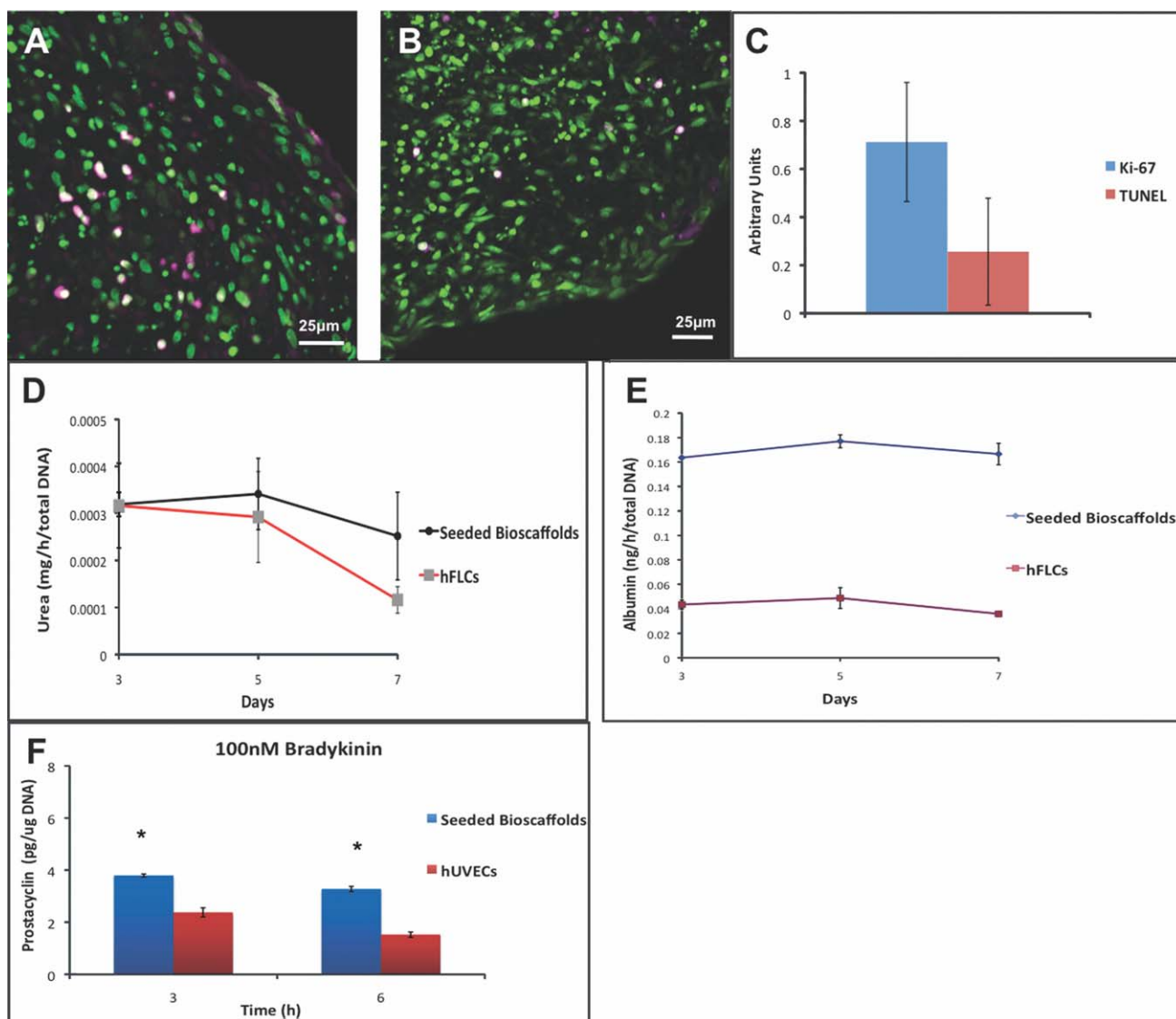


Fig. 6. Quantification of cell proliferation, apoptosis and liver function. Sections of bioscaffolds, 7 days after seeding, were immunostained with anti-Ki67 (purple) (A) and TUNEL (purple) (B); nuclei were labeled with YO-PRO1 (green). Ki67 staining shows a large number of proliferating cells throughout the bioscaffold. (B) TUNEL staining shows only a few apoptotic cells in the seeded bioscaffold. (C) Image analysis of several sections shows significantly higher cell proliferation than apoptosis ( $P = 0.033$ ). (D) (E) Analysis of urea and albumin concentrations in the culture medium shows higher urea and albumin secretion by hFLCs seeded in the liver bioscaffolds than hFLCs seeded in petri dishes ( $P = 0.002$ ;  $P = 0.0006$ ). (F) Determination of 6-keto-PGF<sub>1 $\alpha$</sub>  concentrations in the culture medium shows higher secretion by EC in the bioscaffold than in petri dishes at 3 and 6 hours with 100nM of bradykinin ( $P = 0.033$ ).

hFLC preparations and could have engrafted in the bioscaffolds like hematopoietic cells were not detected (Supporting Information Fig. 5), whereas mesenchymal/stromal cells were observed in the parenchyma of the bioscaffolds.

Functional assessment showed significantly higher urea and albumin concentrations in the culture medium of the seeded bioscaffold than hFL cells in culture dishes ( $P = 0.002$ ;  $P = 0.0006$ ) (Fig. 6D,E). Similarly, ECs in the bioscaffold secreted significantly higher amounts of prostacyclin (PGI<sub>2</sub>) than hUVECs cultured in petri dishes ( $P = 0.033$ ) (Fig. 6F).

## Discussion

One of the major challenges for tissue engineering is to produce large volume tissues and organs for clinical applications. Attempts made to bioengineer liver tissues faced challenges that include cell sourcing, efficient cell seeding, vascularization of the engineered tissue, and provision of authentic cues for tissue development. The present research was aimed at developing a technology that will provide authentic liver microarchitecture and ECM, including the macrovascular and microvascular structures. To do so, we

presented here a method of decellularization that was used to fabricate a naturally derived whole-organ bioscaffold. We used the vascular channels as a conduit for reseeding endothelial and hFL cells inside the bioscaffold. The bioscaffold provided spatial information for cell localization and engraftment, and supported cellular proliferation and phenotype maintenance. These results offer a potential technique for fabrication of human liver tissue that can be readily transplanted into host animals or used for studies of liver cell biology, physiology, toxicology, and drug discovery with further development.

Previously, decellularization of tissue was performed by submersion of the tissue within a detergent solution under agitation to allow cell removal in bulk from the surface of the tissue moving inward.<sup>24</sup> These approaches were successful for decellularization of smaller samples (up to 5 mm in thickness), whereas in thicker specimens the core of the tissue remained cellular. To circumvent this limitation, we took advantage of the native liver vascular network by perfusing the detergent through this network and distributing it throughout the entire liver. This gentle procedure preserves the architecture of the liver matrix and vascular system.<sup>25,26</sup> The choice of detergent for the production of whole organ bioscaffolds using perfusion may also impact the preservation of important biochemical cues. Strong ionic detergents such as SDS facilitate rapid removal of cells from dense tissues and can yield a functional bioscaffold<sup>13</sup> but they may damage some ECM components.<sup>27</sup> Therefore, we opted to use a mild nonionic detergent, Triton X-100. We found that this detergent could successfully decellularize the whole liver, kidney, lungs, spleen, pancreas and small intestine by the removal of ~97% of cellular DNA.<sup>28</sup> These studies highlight the utility of perfusion decellularization to generate whole organ bioscaffolds with significant potential for organ bioengineering.

Typically, neovascularization of bioengineered tissues was addressed by supplementing cells with angiogenic growth factors<sup>29,30</sup> or fabricating scaffolds from synthetic material that allowed micro-patterning of vascular tree-like structures.<sup>31</sup> When growth factors are used alone, they tend to create only a microvasculature consisting of small and fragile capillaries, and therefore this technique is only applicable for the engineering of smaller size tissues. An alternative fabrication method is using a micropatterning technique that can be scaled up to larger sizes by modular construction. However, currently this method cannot replicate the progressive complexity and ECM composition of the native liver vascular tree.<sup>32</sup> The bioscaffolds generated from whole

livers produced via our decellularization method retain the complexity of multiple size vessels that can deliver fluids from the larger vena cava or the portal vein and reach each individual liver lobule.

An additional advantage of this method is the retention of important ECM molecules required for site-specific engraftment and/or differentiation of different cell types that are present in the liver. Prior research showed that liver-specific stem cells can be isolated<sup>18,33</sup> and differentiated to hepatic fate.<sup>34</sup> We used hFLCs in combination with hUVECs to recellularize the bioscaffolds, compared with adult hepatocytes used in many previous studies. Adult hepatocytes are larger and susceptible to mechanical stresses, resulting in lower seeding and functional efficiencies. The advantage of seeding fetal liver cells is that they contain large numbers of hepatic progenitors<sup>18,33</sup> that can give rise to hepatocytes, biliary epithelial cells and EC. On the other hand, the progenitors require specific cues to direct them to their native niches in the tissue and to support their growth and differentiation.<sup>35,36</sup> Preservation of ECM molecules and GAGs at their correct locations within the acellular bioscaffold provides these cues. Detection of CK19<sup>+</sup>/CK18<sup>-</sup>/ALB<sup>-</sup> tubular structures as well as clusters of ALB<sup>+</sup>/CK18<sup>+</sup> cells in the parenchyma suggests that the bioscaffold is able to support the differentiation of the fetal hepatoblasts into biliary and hepatocytic lineages, respectively. Thus, the use of the decellularized liver bioscaffold provides not only a three-dimensional vascularized scaffold for nutrient delivery, but also retains the environmental cues necessary for progenitor hepatic and endothelial cells to grow, differentiate and maintain functionality.<sup>35-37</sup>

A major obstacle in producing large-volume tissues is the delivery of adequate numbers of cells to the entire thickness of the tissue. Commonly used methods for cell seeding into scaffolds employ static, dynamic, or perfusion bioreactor seeding,<sup>38</sup> resulting in seeding of cells that can only penetrate several millimeters below the surface, with further engraftment dependent on active migration of the cells. Alternatively, previous methods to recellularize organ scaffolds have relied heavily on direct cell injection, that damaged the scaffold microarchitecture and produced heterogeneous scaffold seeding.<sup>13</sup> The perfusion method introduced here supports cell infusion through the vascular network and deposition throughout the thickness of the bioscaffold, achieving greater seeding efficiency without compromising the integrity of the bioscaffold. Furthermore, by accessing different vessels that feed into the liver, we were able to deliver cells selectively to different compartments of the liver tissue. EC delivered

through the vena cava selectively seeded larger and smaller blood vessels up to the pericentral area of the liver lobule, without reaching the periportal space of the lobule where the final branching vessels of portal vein are located (Fig. 4A). On the other hand, cells seeded through the portal vein, which delivers blood from the intestine and other organs to the liver,<sup>39</sup> reached predominantly the periportal area of the liver lobule without extensive penetration to its pericentral space. These ECs cover the entire circumference of a vascular channel and maintained cell-cell junctions (Fig. 4E and Supporting Information Fig. 3A). We were able to confirm this “selective” seeding by delivering fluorescently-labeled ECs through the portal vein and fluorescent beads via the vena cava in the same bioscaffold, showing that they reached discrete locations in the liver lobule. Thus, simultaneous utilization of both vascular routes for cell seeding enables complete access to the entire length of the vascular network, which has an essential importance for prevention of blood clotting and ultimately failure to transplant the bioengineered liver. Accordingly, we showed that endothelialized bioscaffolds exhibited significant reduction in the presence and adhesion of platelets, compared with unseeded bioscaffolds (Fig. 4F). Yet, further improvement to complete endothelialization of every blood vessel and capillary of the bioscaffold will require larger numbers of ECs and longer bioreactor pre-conditioning time.

Recent studies by Ott et al.<sup>13,40</sup> and Uygun et al.<sup>41</sup> documented the decellularization of rat hearts,<sup>13</sup> lungs,<sup>40</sup> and livers,<sup>41</sup> respectively, using the same perfusion method. The authors used young animal (rat) cells or human cell lines for recellularization experiments. These cells can sustain greater physical and chemical (hypoxia, toxic metabolites, etc.) insults than primary human cells that were used in the current study. The use of primary human cells to recellularize the bioscaffolds provides a clinical application of organ bioengineering.

Delivery of hFLCs through the same vascular access (vena cava and portal vein) resulted in hepatoblasts and biliary epithelial cells in the parenchyma of the bioscaffold. This result is intriguing because of the experimental data that indicated that the vascular network is intact after decellularization. A possible explanation for this result may be that some areas within the vascular walls have very thin and/or disrupted matrix that can be penetrated by cells. This may also explain the progressive leakage of FITC-labeled dextran particles from the vascular channels to the acellular liver parenchyma after 5–10 minutes of constant perfusion. Another explanation is that the seeded cells

use selective matrix binding and penetration through the vascular channels. Although it is possible that both mechanisms are involved, more detailed experiments are needed in order to fully understand the biology behind these cellular behaviors. Fabrication of intact whole-organ bioscaffolds offers a promising approach for solid organ bioengineering. The three-dimensional ECM, with preserved microarchitecture and patent vascular structures, allows repopulation of the bioscaffolds with EC in the vascular channels and liver cells in the parenchyma. Moreover, it supports seeding with large numbers of human liver progenitor cells that preserve their phenotype, are able to proliferate, partially differentiate and are functional (urea and albumin secretion by the hepatoblasts and prostacyclin secretion by the hUVECs). Thus, the bioscaffolds have the potential for accurate reconstruction of liver tissue, by allowing authentic cell-cell and cell-matrix interactions, which are essential for cell differentiation and maintenance of specialized functions. In our view, these liver bioscaffolds have the capability to become a superior liver cell culture system for pharmacology, toxicology and drug discovery, closely mimicking the native three-dimensional structure of liver tissue. The bioscaffold may also prove as a good tool to study normal tissue and organ development as well as liver pathology. Ultimately, this technology may bring us closer to the ultimate goal of providing bioengineered livers for transplantation.

**Acknowledgment:** We thank Dr. Mark Puder and Dr. Ian Alwayn for their assistance with liver anatomy and dissection techniques. We would also like to thank Gil Palchik for assistance with the confocal microscopy and Dr. Ben Harrison for his custom made polyvinyl fluorescent beads. We want to thank Perrin Larton and Advanced BioResources Inc. for their generous help and supply of human fetal livers. We would also like to thank Dr. Lola Reid from the University of North Carolina at Chapel Hill for her invaluable advice for optimizing the experimental conditions for the human fetal liver cells. We would like to thank Dr. Randall McClelland from SciKon Innovation, Inc. and Will Plentl from Zen-Bio, Inc. for their exceptional technical and material assistance in this project. We also want to thank Dr. Mark Furth and Dr. Koudy Williams for their critical review of the manuscript.

## References

1. Zacchi V, Soranzo C, Cortivo R, Radice M, Brun P, Abatangelo G. In vitro engineering of human skin-like tissue. *J Biomed Mater Res* 1998; 40:187–194.
2. Kaushal S, Amiel GE, Guleserian KJ, Shapira OM, Perry T, Sutherland FW, et al. Functional small-diameter neovessels created using endothelial progenitor cells expanded ex vivo. *Nat Med* 2001;7:1035–1040.

3. Atala A, Bauer SB, Soker S, Yoo JJ, Retik AB. Tissue-engineered autologous bladders for patients needing cystoplasty. *Lancet* 2006;367:1241-1246.
4. Griffith LG, Naughton G. Tissue engineering--current challenges and expanding opportunities. *Science* 2002;295:1009-1014.
5. Folkman J, Hochberg M. Self-regulation of growth in three dimensions. *J Exp Med* 1973;138:745-753.
6. De Coppi P, Delo D, Farrugia L, Udompanyanan K, Yoo JJ, Nomi M, et al. Angiogenic gene-modified muscle cells for enhancement of tissue formation. *Tissue Eng* 2005;11:1034-1044.
7. Hollister SJ. Porous scaffold design for tissue engineering. *Nat Mater* 2005;4:518-524.
8. Levenberg S, Rouwkema J, Macdonald M, Garfein ES, Kohane DS, Darland DC, et al. Engineering vascularized skeletal muscle tissue. *Nat Biotechnol* 2005;23:879-884.
9. Griffith CK, Miller C, Sainson RC, Calvert JW, Jeon NL, Hughes CC, et al. Diffusion limits of an in vitro thick prevascularized tissue. *Tissue Eng* 2005;11:257-266.
10. Kaihara S, Borenstein J, Koka R, Lalan S, Ochoa ER, Ravens M, et al. Silicon micromachining to tissue engineer branched vascular channels for liver fabrication. *Tissue Eng* 2000;6:105-117.
11. Badylak SF. The extracellular matrix as a scaffold for tissue reconstruction. *Semin Cell Dev Biol* 2002;13:377-383.
12. Yoo JJ, Meng J, Oberpenning F, Atala A. Bladder augmentation using allogenic bladder submucosa seeded with cells. *Urology* 1998;51:221-225.
13. Ott HC, Matthiesen TS, Goh SK, Black LD, Kren SM, Netoff TI, et al. Perfusion-decellularized matrix: using nature's platform to engineer a bioartificial heart. *Nat Med* 2008;14:213-221.
14. Zandonella C. Tissue engineering: the beat goes on. *Nature* 2003;421:884-886.
15. Chen HC, Hu YC. Bioreactors for tissue engineering. *Biotechnol Lett* 2006;28:1415-1423.
16. Radisic M, Yang L, Boublik J, Cohen RJ, Langer R, Freed LE, et al. Medium perfusion enables engineering of compact and contractile cardiac tissue. *Am J Physiol Heart Circ Physiol* 2004;286:H507-H516.
17. Arbiser JL, Moses MA, Fernandez CA, Ghiso N, Cao Y, Klauber N, et al. Oncogenic H-ras stimulates tumor angiogenesis by two distinct pathways. *Proc Natl Acad Sci U S A* 1997;94:861-866.
18. Schmelzer E, Zhang L, Bruce A, Wauthier E, Ludlow J, Yao HL, et al. Human hepatic stem cells from fetal and postnatal donors. *J Exp Med* 2007;204:1973-1987.
19. Lin P, Chan WC, Badylak SF, Bhatia SN. Assessing porcine liver-derived biomatrix for hepatic tissue engineering. *Tissue Eng* 2004;10:1046-1053.
20. Natsume M, Tsuji H, Harada A, Akiyama M, Yano T, Ishikura H, et al. Attenuated liver fibrosis and depressed serum albumin levels in carbon tetrachloride-treated IL-6-deficient mice. *J Leukoc Biol* 1999;66:601-608.
21. Yasuda M, Shimizu I, Shiba M, Ito S. Suppressive effects of estradiol on dimethylnitrosamine-induced fibrosis of the liver in rats. *HEPATOLOGY* 1999;29:719-727.
22. Sageae M, Sato E, Hayashi Y, Tanaka E, Mori H, Kawai T, et al. Monochromatic polycapillary imaging utilizing a computed radiography system. *Igaku Butsuri* 2004;24:78-85.
23. Haruna Y, Saito K, Spaulding S, Nalesnik MA, Gerber MA. Identification of bipotential progenitor cells in human liver development. *HEPATOLOGY* 1996;23:476-481.
24. Badylak SF. Xenogeneic extracellular matrix as a scaffold for tissue reconstruction. *Transpl Immunol* 2004;12:367-377.
25. Martinez-Hernandez A, Amenta PS. The hepatic extracellular matrix. I. Components and distribution in normal liver. *Virchows Arch A Pathol Anat Histopathol* 1993;423:1-11.
26. Martinez-Hernandez A, Amenta PS. The hepatic extracellular matrix. II. Ontogenesis, regeneration and cirrhosis. *Virchows Arch A Pathol Anat Histopathol* 1993;423:77-84.
27. Samouillan V, Andurand-Lods J, Lamure A, Maurel E, Lacabanne C, Gerosa G, et al. Thermal analysis characterization of aortic tissues for cardiac valve bioprostheses. *J Biomed Mater Res* 1999;46:531-538.
28. Baptista PM, Orlando G, Mirmalek-Sani SH, Siddiqui M, Atala A, Soker S. Whole organ decellularization - a tool for bioscaffold fabrication and organ bioengineering. *Conf Proc IEEE Eng Med Biol Soc* 2009;1:6526-6529.
29. Isner JM, Asahara T. Therapeutic angiogenesis. *Front Bioscience* 1998;3:e49-e69.
30. Borsig C, Storrie H, Benesch-Lee F, Shvartsman D, Cezar C, Lichterman JW, et al. Functional muscle regeneration with combined delivery of angiogenesis and myogenesis factors. *Proc Natl Acad Sci U S A* 2010;107:3287-3292.
31. Shen JY, Chan-Park MB, He B, Zhu AP, Zhu X, Beuerman RW, et al. Three-dimensional microchannels in biodegradable polymeric films for control orientation and phenotype of vascular smooth muscle cells. *Tissue Eng* 2006;12:2229-2240.
32. Kassab GS. Scaling laws of vascular trees: of form and function. *Am J Physiol Heart Circ Physiol* 2006;290:H894-H903.
33. Shafritz DA, Oertel M, Menthe A, Nierhoff D, Dabeva MD. Liver stem cells and prospects for liver reconstitution by transplanted cells. *HEPATOLOGY* 2006;43(2 Suppl 1):S89-S98.
34. Lee KD, Kuo TK, Whang-Peng J, Chung YF, Lin CT, Chou SH, et al. In vitro hepatic differentiation of human mesenchymal stem cells. *HEPATOLOGY* 2004;40:1275-1284.
35. Suzuki A, Iwama A, Miyashita H, Nakauchi H, Taniguchi H. Role for growth factors and extracellular matrix in controlling differentiation of prospectively isolated hepatic stem cells. *Development* 2003;130:2513-2524.
36. McClelland R, Wauthier E, Uronis J, Reid L. Gradients in the liver's extracellular matrix chemistry from periportal to pericentral zones: influence on human hepatic progenitors. *Tissue Eng Part A* 2008;14:5-70.
37. Brown SE, Guzelian CP, Schuetz E, Quattrochi LC, Kleinman HK, Guzelian PS. Critical role of extracellular matrix on induction by phenobarbital of cytochrome P450 2B1/2 in primary cultures of adult rat hepatocytes. *Lab Invest* 1995;73:818-827.
38. Burg KJ, Holder WD Jr, Culberson CR, Beiler RJ, Greene KG, Loeb-sack AB, et al. Comparative study of seeding methods for three-dimensional polymeric scaffolds. *J Biomed Mater Res* 2000;51:642-649.
39. Boyer T, Wright T, Manns M. Zakim and Boyer's Hepatology: A Textbook of Liver Disease. 4th ed. Saunders, 2003.
40. Ott HC, Clippinger B, Conrad C, Schuetz C, Pomerantseva I, Ikonomou L, et al. Regeneration and orthotopic transplantation of a bioartificial lung. *Nat Med* 2010;16:927-933.
41. Uygun BE, Soto-Gutierrez A, Yagi H, Izamis ML, Guzzardi MA, Shulman C, et al. Organ reengineering through development of a transplantable recellularized liver graft using decellularized liver matrix. *Nat Med* 2010;16:814-820.
42. Nagai N, Hosokawa M, Itohara S, Adachi E, Matsushita T, Hosokawa N, et al. Embryonic lethality of molecular chaperone hsp47 knockout mice is associated with defects in collagen biosynthesis. *J Cell Biol* 2000;150:1499-1506.